Empirical Valence Bond Theory Studies of the $CH_4 + Cl \rightarrow CH_3 + HCl$ Reaction

Balázs Hornung,[1] Jeremy N. Harvey,[2] Thomas J. Preston,[1] Greg T. Dunning[1] and Andrew J. Orr-Ewing[1*]

[1] School of Chemistry, University of Bristol, Cantock's Close, Bristol, BS8 1TS, United Kingdom

[2] Department of Chemistry, KU Leuven, Celestijnenlaan 200F, B-3001, Leuven (Heverlee), Belgium

* Author for correspondence:

e-mail: a.orr-ewing@bristol.ac.uk

tel: +44 117 9287672

Abstract

We report a theoretical investigation of the CH_4 + Cl hydrogen abstraction reaction in the framework of empirical valence bond (EVB) theory. The main purpose of this study is to benchmark the EVB method against previous experimental and theoretical work. Analytical potential energy surfaces for the reaction have been developed on which quasi-classical trajectory calculations were carried out. The surfaces agree well with *ab initio* calculations at stationary points along the reaction path and dynamically relevant regions outside the reaction path. The analysis of dynamical data obtained using the EVB method, such as vibrational, rotational and angular distribution functions, shows that this method compares well to both experimental measurements and higher-level theoretical calculations, with the additional benefit of low computational cost.

Introduction

Theoretical and computational investigation of the mechanisms of chemical reactions is a rapidly evolving field that now spans a range of scales from elementary reactions of small molecules to biological catalysis. Since the classic work of Eyring and Polanyi,[1-3] enormous progress has been made; the present day witnesses a rapid expansion in the chemical systems accessible to quantitative study, and considerable sophistication of the theoretical methods applied to the field of reaction dynamics.[4-5] One prerequisite of any meaningful dynamical study is an accurate knowledge of the forces acting in the reactive system, which still presents a considerable challenge even for elementary reactions. In most cases, this task amounts to constructing a potential energy surface (PES) of sufficient quality for accurate simulation of atomic motions.

An ideal PES for dynamical calculations describes correctly the forces experienced in all of the atomic degrees of freedom. Developing such a global PES requires many reliable electronic structure calculations, and high-level *ab initio* electronic structure theory methods are usually preferred. In practice, it is often prohibitively computationally expensive to obtain a global PES, save for systems

consisting of only a few atoms, using the current high level *ab initio* methods. Another crucial aspect of constructing PESs that are continuous functions of all atomic coordinates is that of the accurate representation and interpolation of the discrete *ab initio* energies obtained from electronic structure calculations. A popular approach is to fit the *ab initio* energies with a suitably chosen set of analytical functions.[6-7] This method works best if only a few atoms are included in the system.

Permutationally invariant polynomial fitting, developed by Bowman and co-workers,[6, 8-10] takes into account the chemical identity of the atoms involved in the reaction, hence reducing the computational effort of fitting *ab initio* energy points. This method, coupled with state-of-the-art electronic structure energies, has been successfully applied to many reactions involving systems with 3 to 8 atoms.[11-12] This approach, however, requires many *ab initio* points, usually on the order of 10,000 to 50,000 depending on the size of the system.

Another popular approach to fit potential energy surfaces is to invoke accurate interpolation schemes without using fitted energy functions. The reproducing kernel Hilbert Space (RKHS) interpolation operates on a set of tabulated *ab initio* points. The computational demand usually scales with 10^n, where n is the number of dimension, hence it is a practically feasible method for systems of 3-4 atoms.[13-14] The modified Shephard interpolation[15-16] approximates the energy of a required geometry by a weighted combination of Taylor expansions from the vicinity of that point. The number of *ab initio* point required by this interpolation method scales better than the RKHS method with the size of the system.

As the number of atoms increases, new methodologies can combat unfavourable scaling. It is sometimes feasible to divide the system into smaller subsystems, as in the fragment molecular orbital and systematic molecular fragmentation scheme of Collins *et al*.[17-18] High level *ab initio* methods describe interactions within the subsystems while simpler functions determine forces between them. When the size of the system exceeds about ten atoms, constructing a fully *ab initio* global PES becomes practically impossible; each single-point calculation takes additional time, and each new degree of

freedom makes for larger geometry searches. Simulating larger systems, as in condensed-phase biochemistry studies, instead typically uses molecular mechanics force fields. These force fields are usually incapable of describing the forming and breaking of chemical bonds. To address this limitation, Warshel developed the empirical valence bond (EVB) method in which the PES regions corresponding to the reactants and product are approximated by molecular mechanics force fields, and the change in energy associated with the variation of connectivity is accounted for using coupling elements.[19-20] The EVB method was originally used to explain experimental observations in protein reactions, but was later extended to smaller reactive systems. A closely related method, the multiconfiguration molecular mechanics approach combines the EVB formalism with sophisticated interpolation algorithms.[21]

Our current effort applies the EVB formalism to the reaction between methane and a chlorine atom, which has been extensively studied experimentally and theoretically using some of the techniques described above.[22-24] This attention in part reflects the importance of the Cl + CH_4 reaction in the chemistry of the Earth's atmosphere, but it also serves as a benchmark system for the dynamics of reactions of polyatomic molecules. Since the measurement of the first state-resolved differential cross sections,[25] which quantify product flux as a function of scattering angle, further experiments have explored the effects of collision energy on reaction cross sections and product scattering.[26] Reactive scattering dynamics have proven to be sensitive to the translation and internal excitation of the methane. The outcome of the reaction can be controlled by vibrational excitation of specific bonds or vibrational modes;[27-29] for example, excitation of the symmetric stretch-bend combination promotes the reaction twenty times more efficiently than exciting the antisymmetric stretch-bend combination.[30] However, Liu and coworkers showed that excitation of the CH stretch in the CD_3H molecule facilitated the reaction to a lesser extent than increasing the collision energy by a corresponding amount.[31] This observation is contrary to the predictions of the Polanyi rules. Czakó and Bowman showed that van der Waals forces between the two colliding fragments, which are absent in the Polanyi rules framework, account for this surprising result.[32] The alignment of the

methane molecular framework can also drastically influence the product angular distribution and polarization.[28, 33]

Despite its relatively small size, the explicit treatment of all twelve internal degrees of freedom of the PES on which the CH_4 + Cl reaction occurs presents considerable challenges for both constructing the PES and running dynamical calculations. Reduced-dimensionality approaches have proved successful: three- and four-dimensional models were employed by Nyman and co-workers[34-36] in which the reactive C—H—Cl coordinate (described by a London-Eyring-Polanyi-Sato (LEPS) potential), the umbrella motion of the CH_3 group and the coupled motions of the CH_4 reactant were taken into account. Quantum scattering calculations on these model PESs reproduced some of the experimental observations, such as the characteristics of the differential cross sections. Reduced dimensionality quantum scattering studies were also carried out by Clary and coworkers in which the two spin–orbit states of the system were considered.[23-24, 37]

Treatment of all degrees of freedom of the reaction is feasible with classical scattering methods. For example, Troya and coworkers used a full-dimensional semi-empirical PES to perform quasi-classical-trajectory (QCT) calculations.[38-39] The first global pre-calculated *ab initio* PES used in QCT calculations was reported by Castillo *et al.*[40] Their approach used QCISD(T)/aug-cc-pVTZ//QCISD/cc-pVTZ calculations to determine the energies of the separated reactants and products and those of the pre- and post-reaction complexes. The other regions of the PES were calculated using the interpolation algorithms of Collins and co-workers.[41-43] The most accurate global PES for this system is that computed by Czakó and Bowman.[32, 44] In their study, high level, composite electronic energies were calculated at the E[UCCSD(T)/aug-cc-pVDZ] + E[AE-UMP2/aug-cc-pCVTZ] – E[UMP2/aug-cc-pVDZ] level. Focal-point analysis and implicit treatment of the spin-orbit interaction were also invoked to produce an accurate PES. The PES was subsequently fitted with permutationally invariant polynomials. The QCT calculations reproduced the experimental rotational distribution of the HCl within the uncertainties of the experiment. Moreover, Bowman and Czakó succeeded in explaining how the

excitation of various normal modes of the CH_4 steers the outcome of the reaction, as observed experimentally by Liu and coworkers.[27, 29]

On-the-fly direct dynamics calculations, an alternative to fitting a reactive PES, compute local information about the fully dimensional PES at each step of the trajectory. As a result, the reaction always stays on the exact *ab initio* PES. However, the energy and gradients have to be determined at each step, usually by low level electronic structure methods such as Hartree-Fock or density functional theory. Fully dimensional on-the-fly classical dynamics calculations were carried out for the CH_4 + Cl reaction using a semi-empirical model Hamiltonian by Troya *et al.*[38, 45] and using the Hartree–Fock /6-31G level of theory by Rudić *et al*.[46] A similar approach was adopted by Greaves *et al*. who investigated the transferability of model Hamiltonians between related reactions.[39]

The purpose of the current study is to test the EVB description of a PES generated from high level *ab initio* electronic structure calculations. The EVB fit to obtain a global PES requires fewer *ab initio* points than the alternative PES fitting methods described above. By concentrating on a well-studied reaction, we examine whether the accuracy of the EVB fit is adequate to describe the reactive scattering dynamics. The outcomes therefore have implications for application of the EVB method to reactions in larger systems.[47-48] The paper is organized as follows. The details of the electronic structure calculations are first provided. The procedure to obtain molecular mechanics force field parameters and reactive EVB PES is then described, along with the details of the QCT calculations. The result of these calculations are analysed and compared to previous experimental and theoretical works. Finally, the value of extending the EVB method to other, more complicated, systems is considered.

Methods

Electronic Structure Calculations

The reactant, product and transition state structures for the $CH_4 + Cl \rightarrow CH_3 + HCl$ reaction were optimized using restricted open shell second order Møller–Plesset perturbation theory (RMP2)

employing Pople's 6-311G(d,p) basis set. Explicitly correlated coupled-cluster singles, doubles and perturbative triples (CCSD(T)-F12B)[49] energies with the aug-cc-pVTZ[50] basis set on the H and C atoms and aug-cc-pV(T+d)Z on the Cl atom (and appropriate auxiliary fitting basis sets) were calculated for these geometries. Using the explicitly correlated method, basis set superposition error is negligible,[49] hence further corrections for this effect were not carried out. Rigid scans were performed along relevant internal coordinates of the separated CH_4, CH_3 and HCl reactants and products to fit the molecular mechanics force field energy terms for these species. The energies along these scans were computed at the CCSD(T)-F12B/aug-cc-VTZ level of theory, starting from initial optimum structures obtained at the RMP2/6-311G(d,p) level. Spin-orbit interactions were neglected for all *ab initio* calculations; reaction of spin-orbit excited Cl($^2P_{1/2}$) with methane requires a non-adiabatic transition from a repulsive PES to the ground-state Cl($^2P_{3/2}$) + CH_4 surface.[22] The MOLPRO suite of codes was used to perform all of the electronic structure calculations.[51] For testing purposes, vibrational frequencies were calculated for HCl, CH_3, CH_4 and the transition state at the CCSD(T)-F12B/aug-cc-pVTZ level at the geometries optimised at the same level using numerical gradients.

Two sets of points on the overall reactive Cl + CH_4 potential energy surface were generated to provide fitting sets for the EVB potential. In the first case, points were obtained on and around the minimum energy path to reaction. Fixed values of the Cl-H and H-C distances were chosen, then the remaining degrees of freedom were optimized, at the RMP2/6-311G(d,p) level of theory, within the C_{3v} point group which resulted in roughly 300 *ab initio* points. The CCSD(T)-F12B/aug-cc-pVTZ energies at the structures obtained from this two-dimensional scan formed the basis for a first fitted EVB surface, which we label EVB(1). The second set of points comprised structures obtained by randomly sampling reactive trajectories. For these additional geometries, CCSD(T)-F12B/aug-cc-pVTZ calculations were also performed, and the resulting set of energies was used to fit a second-generation EVB surface, that we label EVB(2). The details of the sampling are given in the next section.

Construction of the reactive EVB Potential

The EVB framework divides configuration space into regions corresponding to the reactants, intermediates and products, which are each treated as diabatic states.[19-20] Their potential energies are computed approximately using molecular mechanics force field expressions, based on sums of terms that depend on the value of chemically relevant descriptors such as bond stretches, angle bends, and dihedral torsions. These molecular mechanics potential energies constitute the diagonal elements of the EVB matrix. For a given structure, the first element V_{11} corresponds to the energy of the system, obtained using a force-field in which the atomic connectivity is that of the reactants, CH_4 + Cl. For the same structure, the four diagonal elements V_{22},…,V_{55} are the energies computed using a product-like forcefield with CH_3 + HCl connectivity. As there are four hydrogen atoms, there are four possible product connectivities and hence four different diagonal elements, though of course the same molecular mechanics parameters are used for each of them. The molecular mechanics energies for reactant and product connectivities refer to different energy scales. In order to make them comparable, an offset energy E_0 is chosen such that the offset between the V_{11} and V_{22} diabatic potentials at the corresponding reactant and product optimum structures corresponds to the CCSD(T)-F12B reaction energy. The off-diagonal elements V_{ab}=V_{ba}, $a \neq b$, describe the coupling between the diabatic states. Given that we are interested in modelling the reaction Cl + $CH_4 \rightarrow$ HCl + CH_3, and that hydrogen exchange between HCl and CH_3 in the product channels is unlikely, we chose to set all off-diagonal elements V_{ab}, a, b >1, to zero. The adiabatic EVB energy at any geometry is obtained by solving the eigenvalue problem (1) and choosing the lowest energy eigenvalue.

$$\begin{bmatrix} V_{11} & V_{12} & V_{13} & V_{14} & V_{15} \\ V_{21} & V_{22}+E_0 & 0 & 0 & 0 \\ V_{31} & 0 & V_{33}+E_0 & 0 & 0 \\ V_{41} & 0 & 0 & V_{44}+E_0 & 0 \\ V_{51} & 0 & 0 & 0 & V_{55}+E_0 \end{bmatrix} \underline{c} = E\underline{c}. \qquad (1)$$

The EVB gradient is calculated according to

$$\nabla E = \sum_{ab} c_a c_b \nabla V_{ab}, \tag{2}$$

where $\underline{c}$ is the normalized eigenvector belonging to the lowest eigenenergy E.[52] In the present study, new force fields were constructed for the reactants and products. The included energy terms account for the bonded and for the non-bonded interactions. The molecular mechanics energy terms for bonded atoms were parameterized using the *ab initio* geometries and energies described above. We chose Morse potentials to describe the energy associated with the atom-atom stretching. Quartic bending terms account for bending motions, and Wilson-type improper torsions describe the out-of-plane motion of the H-atoms of the methyl fragment.[53] The stretch-bend interaction proved to be negligible, hence it is not included in the force fields. The four-parameter Buckingham-Corner potential function approximates the non-bonded interactions.[54]

The coupling term that connects the reactant and product states can be chosen in several different ways, e.g. it can be a function of all the nuclear degrees of freedom.[21, 55] We have however found that a simpler function, that depends only on a smaller number of internal coordinates relating to the atoms that change connectivity during the course of the reaction, provides a more than adequate accuracy for the fitted potential.[47] The coupling term employed in this study is a two-dimensional Gaussian function that depends on the reactive C—H and H—Cl distances:

$$V_{ab}(r_{C-H}, r_{H-Cl}) = A \exp\left[-\frac{\left(r_{C-H} - r_{C-H,0}\right)^2}{2\sigma_{C-H}^2} - \frac{\left(r_{H-Cl} - r_{H-Cl,0}\right)^2}{2\sigma_{H-Cl}^2} - c_{C-H-Cl}\left(r_{C-H} - r_{C-H,0}\right)\left(r_{H-Cl} - r_{H-Cl,0}\right) \right]. \tag{3}$$

A is the amplitude of the Gaussian function, and r_{C-H}, r_{H-Cl} are the bond lengths. The parameters $r_{C-H,0}$, $r_{H-Cl,0}$ are the centers, and σ^2_{C-H}, σ^2_{H-Cl} are the widths of the Gaussian function, respectively, whereas c_{C-H-Cl} relates to the angle between the main axis of the coupling term and the $\underline{r}_{C-H}$ vector. Sums of one-dimensional Gaussian functions were also tested as coupling elements, but the 2D functions of Eqn. (3) gave superior quality fits to the *ab initio* surface. In a similar way, we found in our study of the

F + CD_3CN reaction that a two-dimensional Gaussian coupling function provides a better fit to the *ab initio* values.[56]

The parameters of the individual energy terms of the CH_4 and CH_3 molecules were determined by fitting rigid *ab initio* scans along the appropriate internal coordinates. Using these preliminary energy terms, we propagated a molecular dynamics trajectory of each fragment to build a set of random CH_4 and CH_3 geometries. The trajectories were initialised with CH_4 molecules having their ZPE and with a collision energy of 28.0 kJ mol^{-1}. CCSD(T)-F12B energies were obtained at these structures in the range of 21 to 150 kJ mol^{-1}, and used to perform a final fit of the internal force field parameters for the CH_4 and CH_3 species. These parameters were held fixed during all of the subsequent fitting procedures. The HCl stretch parameters were obtained by fitting its CCSD(T)-F12B potential energy curve.

There are four types of non-bonded interactions according to the chemical identity of the atoms in the reactive system, namely C—Cl, H—Cl, C—H, and H—H. The carbon, hydrogen and chlorine atoms were treated identically regardless of whether in a reactant or product species. For example, the interactions between the H atoms in CH_4 and the Cl atom, and between the H atoms in the CH_3 radical and the Cl atom in the HCl molecule were assumed to be identical. Initial parameters for the Buckingham-Corner potential were obtained by fitting *ab initio* energies of randomly arranged CH_4 + H_2, and CH_4 + Cl_2 geometries.

Two reactive EVB potentials were constructed, EVB(1) and EVB(2). For EVB(1), fitting was performed to a set of CCSD(T) energies computed at structures with C_{3v} symmetry. As mentioned above, these structures were obtained from 2-D scans in which the C-H and H-Cl distances were fixed, and the other coordinates optimized using the RMP2 method. Approximately 300 points of this type were used in the fit, ranging in energy from 0 to 150 kJ mol^{-1} relative to separated reactants. The fitting was performed using a modified form of the EVB eigenvalue equation (1), in which only one product connectivity was considered, so that the EVB matrix was only of 2x2 size. An EVB matrix of 5x5 with these parameters returns a PES almost identical to that from the 2x2 matrix.

A single 2D coupling term was used for the off-diagonal element. The parameters of the coupling term and those of the C—H, H—Cl, and C—Cl non-bonded terms were floated. Using a genetic algorithm to explore the fit parameters, we aimed to minimize the square of the difference between the *ab initio* and EVB energies. The energy of the separated reactants was taken as reference, or zero point of the PESs. The weights were the inverse square of the corresponding *ab initio* electronic structure energy. No *ab initio* points had an absolute value below 0.05 kJ mol^{-1} hence the fit was not overly biased towards points close to the asymptote.

$$\chi^2 = \sum_i \left(\frac{E_{EVB,i} - E_{ab\ initio,i}}{E_{ab\ initio,i}} \right)^2 if\ \left| E_{ab\ initio,i} \right| > E_{thresh} \quad (4)$$

A 5x5 EVB matrix of the form of Equation (1) was constructed with the optimized coupling and non-bonding terms from the 2x2 EVB fit to obtain the EVB(1) surface. It is important to note that although the structures used to fit the parameters for the non-bonding terms and the off-diagonal matrix elements of EVB(1) are all of C_{3v} symmetry, this potential is able to describe non-symmetric structures also.

A number of reactive trajectories, which sample non-C_{3v} symmetries as described above, were run on this surface. Random points were selected from these trajectories for which 500 CCSD(T)-F12B/aug-cc-VTZ energies were calculated and subsequently used to fit the EVB(2) potential. In this case, a 5x5 EVB matrix was used in the fitting process, and the H–Cl, H–C, C–Cl van der Waals and coupling parameters were floated. The values of EVB parameters obtained from the fits for both surfaces are reported in the Supporting Information.

The quasi-classical trajectories were run with the VENUS suite of codes[57] interfaced with an EVB module developed in our group. This module calculates the EVB energy and the analytical first derivatives. The second derivatives are calculated numerically when needed. The methane molecule had an initial internal energy corresponding to its zero-point energy (ZPE), which was distributed

among its normal modes *via* orthant sampling.[58-59] The methane molecule was randomly oriented relative to the incoming Cl atom. The impact parameter was randomly sampled in the 0–5 Å interval. The initial Cl–methane separation was set to 5 Å. A time-step of 0.1 fs ensured good energy convergence during the entire course of propagation, which was typically about 700 fs. Specifically, the total (potential plus kinetic) energy was monitored, taking the zero of potential energy as the optimum energy of the separated reactants with respect to the energy of the entrance channel. This was conserved to better than 0.01%, or approx. 0.16 kJ mol^{-1}. Only those reactive trajectories were accepted where both products had at least their ZPE in vibrational energy. We used a histogram binning method to obtain rotational and vibrational quantum numbers to allow ready comparisons with the work of Czakó and Bowman.[32]

Results and Discussion

The computed energetics of stationary points along the reaction pathway are summarized in Figure 1. The CCSD(T)-F12B/aug-cc-pVTZ//RMP2/6-311G(d,p) reaction energy is 21.4 kJ mol^{-1} (5.1 kcal mol^{-1}) which is slightly lower than the value of 25.2 kJ mol^{-1} (6.0 kcal mol^{-1}) reported by Czakó and Bowman.[32, 44] Here, and below, we provide energies in kcal mol^{-1} in parentheses where appropriate to facilitate comparison with the results of this prior study. The transition state lies above the CH_4 + Cl entrance channel by 29.8 kJ mol^{-1} (7.1 kcal mol^{-1}), and its geometric parameters are reported in Table 1. Again, the corresponding TS energy of the accurate surface of Czakó and Bowman is higher, at 31.9 kJ mol^{-1} (7.6 kcal mol^{-1}).[32] These differences are in large part due to our neglect of spin-orbit interactions which lower the energy of the entrance channel by 3.4 kJ mol^{-1} (0.8 kcal mol^{-1}).[22, 32] The methane and Cl atom form a weakly bound pre-reaction complex, the *ab-initio* well depth of which is 1.7 kJ mol^{-1}. A feature corresponding to the post-reaction complex between the methyl radical and the HCl molecule is found at an energy of 11.8 kJ mol^{-1} relative to reactants (or 9.7 kJ mol^{-1} below the products), which is lower than the value established by Czakó and Bowman by 4.2 kJ mol^{-1} (1.0 kcal mol^{-1}). In general, the CCSD(T)-F12B/aug-cc-pVTZ//RMP2/6-311G(d,p) PES compares well to the best of the known PESs.

We used 300 C_{3v} *ab initio* points to fit the EVB(1) surface and a separate set of 500 randomly selected geometry points from reactive trajectories for the EVB(2) surface. The mean unsigned fitting errors were 1.3 kJ mol^{-1} for EVB(1) and 2.6 kJ mol^{-1} for EVB(2) in the 0–150 kJ mol^{-1} energy range. The corresponding error for the EVB(1) fit when compared to the *ab initio* energy points used to fit the EVB(2) surface is 4.2 kJ mol^{-1}, and (coincidentally) the same mean unsigned error is obtained in the reverse comparison of the EVB(2) fit with the *ab initio* energy points used to construct the EVB(1) surface.

Table 1: Ab Initio RMP2/6-311G(d,p), EVB(1) and EVB(2) Transition State and Exit Channel Complex Geometries.[a]

	Transition State				Exit Channel Complex		
	ab initio	EVB(1)	EVB(2)	C&B[g]	EVB(1)	EVB(2)	C&B[g]
R_{Cl-H} / Å	1.414	1.462	1.452	1.437	1.291	1.282	1.282
R_{C-H} / Å [b]	1.433	1.351	1.396	1.403	2.195	2.220	2.274
$R_{C-H(m)}$ / Å [c]	1.085	1.085	1.085	1.083	1.080	1.080	1.081
α / degrees[d]	180.0	180.0	180.0				
β / degrees[e]	100.8	102.5	104.0	101.0			
γ / degrees[f]	116.6	115.4	114.4				

(a) See the insert to Fig. 1 for a representation of the geometric parameters.
(b) C-H distance of the breaking bond.
(c) C-H distance in the methyl moiety.
(d) α is the angle between the breaking C-H bond and the forming H-Cl bond.
(e) β is the angle between a methyl C-H bond and the breaking C-H bond.
(f) γ is the angle between two C-H bonds in the methyl moiety.
(g) PES of Czakó and Bowman from Ref. [44] and Supporting Online Material for Ref. [32].

The EVB fit outcomes are compared with the *ab initio* energies of stationary points in Figure 1. The energy level of the reactants defines the zero of the energy profiles. The EVB and *ab initio* reaction energies are identical *per definitionem*. The transition state structures (see Table 1, with parameters defined in Fig. 1) and energies $E^{\ddagger}$ of EVB(1) and EVB(2), deduced by locating the saddle points on the surfaces, compare well with those obtained from our current electronic structure calculations and with the TS on the Czakó and Bowman PES. There is also good agreement between our calculations and those of Czakó and Bowman for the geometry of the exit-channel complex. The TS is slightly earlier along the reaction pathway in the EVB surfaces than in our *ab initio* calculation.

Energies of the stationary points are obtained as follows on the EVB surfaces. For EVB(1), $E^{\ddagger}$ is 29.4 kJ mol^{-1} (7.0 kcal mol^{-1}), for EVB(2) $E^{\ddagger}$ is slightly higher at 31.9 kJ mol^{-1} (7.6 kcal mol^{-1}), and the *ab initio* result is 29.8 kJ mol^{-1} (7.1 kcal mol^{-1}). The pre-reaction complex has a well depth of -1.76 kJ mol^{-1} (-0.42 kcal mol^{-1}) for EVB (1) and -4.2 kJ mol^{-1} (-1.01 kcal mol^{-1}) for EVB(2). The *ab initio* exit-channel energy well at 11.7 kJ mol^{-1} (2.8 kcal mol^{-1}), is well matched by the EVB(1) value of 11.7 kJ mol^{-1}. The EVB(2) surface, however, predicts the complex has an energy of 15.9 kJ mol^{-1} (3.8 kcal mol^{-1}). The inclusion of more points in the *ab initio* PES around the transition state and exit channel region is expected to improve the goodness of the EVB(2) fit, though it would lead to a biased sampling. Increasing the number of *ab initio* points equally sampled from all possible geometries would considerably increase the computational effort of the electronic structure calculations.

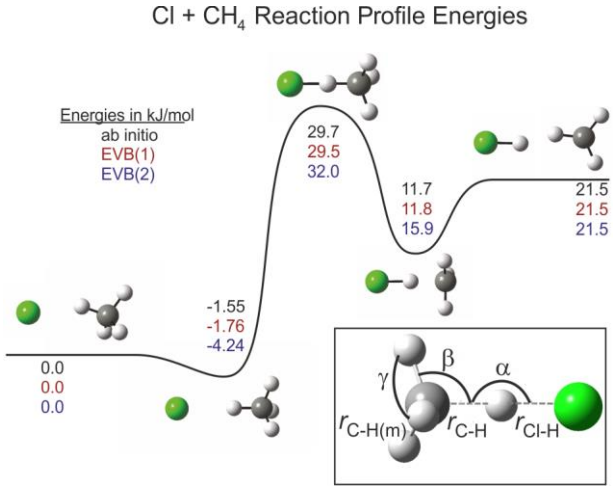

Figure 1: Representation of the energies and structures of stationary points along the reaction pathway for Cl + CH_4 → HCl + CH_3. Energies (in kJ mol^{-1}) of these structures are shown for the CCSD(T)-F12B/aug-cc-pVTZ//RMP2/6-311G(d,p) ab initio *calculations (black) described in the text, and the EVB(1) and EVB(2) PES fits (red and blue respectively), and are specified relative to the energy of separated Cl and CH_4 reactants. The energies do not include zero-point vibrational energy corrections. The boxed insert shows the angle and bond labels used to specify stationary point structures.*

Moving beyond the static properties, we also assess the molecular frequencies, which are a dynamical characteristic of the fitted PESs. The reactant, product and TS frequencies are compared in Tables 2-3. The EVB(1) and EVB(2) frequencies of the CH_4, CH_3 and HCl molecules are identical, due to the construction method of the force fields. The EVB and electronic structure values are in good

agreement: for example, the average deviation between the EVB and *ab initio* CCSD(T)-F12B/aug-cc-pVTZ//RMP2/6-311G(*d,p*) TS frequencies is 5% for EVB(1) and 4% for EVB(2); the agreement is marginally (~1%) poorer when the EVB frequencies are compared to CCSD(T)/aug-cc-pVTZ calculated values from Ref. [39].

Table 2: The CCSD(T)-F12B/aug-cc-pVTZ Ab Initio *and EVB Frequencies of HCl, CH_4 and CH_3 Specified in cm^{-1}.*

	Normal mode	*ab initio*	EVB	Experiment[(a)]
HCl	v_1	2996	3001	2885
CH_4	v_1	3033	3032	2917
	v_2	1569	1545	1534
	v_3	3155	3204	3019
	v_4	1345	1380	1306
CH_3	v_1	3121	3089	3004
	v_2	509	557	606
	v_3	3121	3089	3161
	v_4	1422	1405	1402[(b)]

(a) Values are taken from the NIST Chemistry Webbook[60]
(b) Value for methyl radicals in an H_2 matrix

Table 3: Comparison of Ab Initio (CCSD(T)-F12B/aug-cc-pVTZ//RMP2/6-311G(d,p) and CCSD(T)/aug-cc-pVTZ), EVB(1) and EVB(2) Frequencies (Specified in cm^{-1}) at the Transition State.

Frequency	*CCSD(T)-F12B/aug-cc-pVTZ*	CCSD(T)/aug-cc-pVTZ[(a)]	EVB(1)	EVB(2)
imaginary	1119	973	1190	1251
1	358	350	293	367
2	358	350	293	367
3	498	520	466	425
4	933	886	902	913
5	933	886	902	913
6	1194	1176	1224	1139
7	1433	1407	1421	1410
8	1433	1407	1421	1410
9	3087	3069	3081	3079
10	3249	3238	3240	3244
11	3249	3238	3240	3244

(a) From Ref. [39].

The zero point energies (ZPE) of the reactants, products, the TS and the ZPE corrected reaction energy and barrier height are shown in Table 4. With inclusion of ZPE, the corrected reaction energy is -2.5 kJ mol^{-1}, which with spin-orbit correction would become +0.8 kJ mol^{-1}. In comparison, measured heats of formation of reactants and products combine to give $\Delta_r H_{0K}$ = + 4.6 kJ mol^{-1} (1.1 kcal mol^{-1}).[32] The corrected barrier heights are 9.2 kJ mol^{-1} and 11.7 kJ mol^{-1} for the EVB(1) and EVB(2) surfaces, respectively. The total available energy for the products, when the ZPE is taken into account, is the sum of the corrected reaction energy and the collision energy. At the experimental collision energy of 15.5 kJ mol^{-1} (3.7 kcal mol^{-1}),[22] only 19.7 kJ mol^{-1} is therefore available to be distributed among the internal and relative degrees of freedom of the products. As a consequence, many of the products appear with less than the quantum-mechanically required zero-point vibrational energy. Of the 20,000,000 trajectories we propagate for each surface, 200,000 are reactive, but only 458 on the EVB(1) and 922 on the EVB(2) surface satisfied our zero-point energy criterion. The remainder were rejected. To test the statistical reliability of these trajectories, integral and differential cross sections were calculated using only the half the successful number and compared to the results from the full set. The two sets of results were practically identical.

Table 4: The Zero Point Energies for the Reactants, Products and Transitions State, and Zero Point Energy Corrected Reaction Energy (E_0) and Barrier Height ($E^{\ddagger}$), all Specified in kJ mol^{-1}.[(a)]

	Ab initio [(b)]	EVB(1)	EVB(2)
E_{ZPE}(reactants)	118 (28.1)	119 (28.4)	119 (28.4)
E_{ZPE}(products)	94.0 (22.4)	96.0 (22.9)	96.0 (22.9)
E_{ZPE}(TS)	101 (24.2)	98.6 (23.5)	98.7 (23.6)
E_0(ZPE corrected)	-2.5 (-0.6)	-1.5 (-0.4)	-1.5 (-0.4)
$E^{\ddagger}$(ZPE corrected)	13.2 (3.1)	9.2 (2.2)	11.7 (2.8)

(a) Values in parentheses are specified in kcal mol^{-1}.
(b) CCSD(T)-F12B/aug-cc-pVTZ//RMP2/6-311G(d,p) calculations.

Analysis of trajectories to obtain HCl vibrational distributions confirms that the HCl(v=0) final state is exclusively populated at a collision energy of 15.5 kJ mol^{-1}. Even at the higher collision energy we simulate, E_{coll} = 42.0 kJ mol^{-1}, the HCl(v=1) products at 36.0 kJ mol^{-1} are only just accessible for the

products. At this higher collision energy of 42.0 kJ mol^{-1}, about 1–3% percent of the vibrational population of HCl is in the first excited state.

The HCl(v=0) relative rotational populations obtained from the EVB(1) and EVB(2) surfaces are shown in Figure 2. At E_{coll} = 15.5 kJ mol^{-1} (Fig. 2(a)), the EVB(1) distribution is slightly broader than that resulting from the EVB(2) surface, but the two are otherwise similar. Both reproduce the characteristics of the experimentally observed cold distributions.[61] The most probable experimental j value is unity, whereas the present calculation predicts a somewhat hotter j=2-3 for the peak of the distribution. This discrepancy is small in energy terms (~1 kJ mol^{-1}) and can be explained by inspecting the topography of the exit channel. The wall of the exit channel is steeper with respect to the C—H—Cl bending coordinate on the EVB surfaces than on the *ab initio* PES and in the real system, hence the departing HCl molecule experiences a greater torque that results in a hotter rotational distribution. In addition, this wall is steeper on the EVB(2) than the EVB(1) surface, shifting the rotational distribution at E_{coll} = 42.0 kJ mol^{-1} (Fig. 2(b)) towards higher j values. Computation of additional *ab initio* energies at geometries corresponding to this exit channel region of the PES and a refit of the EVB function parameters might improve the agreement between our trajectory calculation outcomes and the experimental measurements of HCl rotational energies. Nevertheless, our existing fits provide a satisfactory account of this aspect of the reaction dynamics for a modest computational investment in electronic structure calculations.

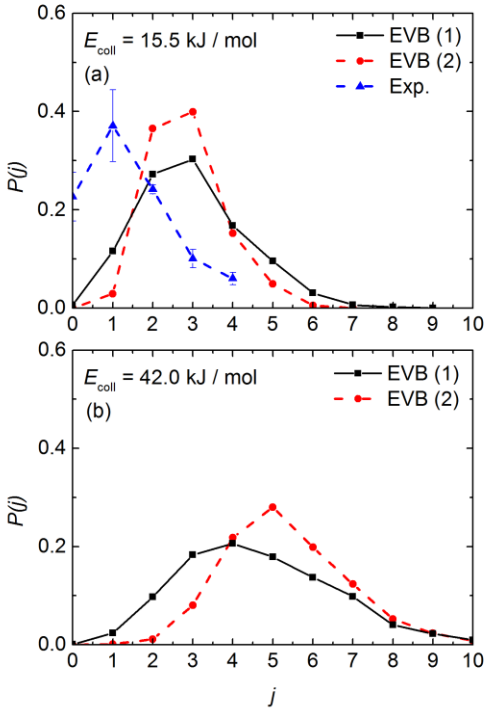

Figure 2: Calculated final rotational distributions of HCl from the CH_4(v=0) + Cl → CH_3(v=0) + HCl(v=0) reaction at a collision energy of (a) 15.5 kJ mol^{-1} and (b) 42.0 kJ mol^{-1}. The distributions were computed using the EVB (1) (black solid squares) and EVB (2) (red solid circles) PESs, and are compared to experimental measurements [Ref. 61]at the lower collision energy (blue triangles).

Differential cross sections, which relate reactive probability to product scattering angle, are shown in Figure for the two EVB surfaces and for experimental results (which probed CH_3(v=0) and averaged over HCl(v=0) rotational levels).[26] The computed differential cross sections are shown at two collisions energies, 15.5 kJ mol^{-1} (Fig. 3(a)) and 42.0 kJ mol^{-1} (Fig. 3(b)). The EVB surfaces show that HCl(v=0) products are predominantly backward scattered, which is in good agreement with experiment at the lower collision energy.[26] There is only about 5.9 kJ mol^{-1} and 3.8 kJ mol^{-1} excess energy above the zero point energy corrected barrier at E_{coll} = 15.5 kJ mol^{-1} on the EVB(1) and EVB(2) surfaces, respectively. Lacking much energy to spare, surmounting the reaction barrier requires the initial relative linear momentum of the collision partners to be aligned along the reactive C—H bond vector (the reaction

coordinate). As a consequence of the linear transition state, the relative momentum of the products will likely be oriented antiparallel to that of the reactants, resulting in the backwards scattering shown in Fig. 3(a).

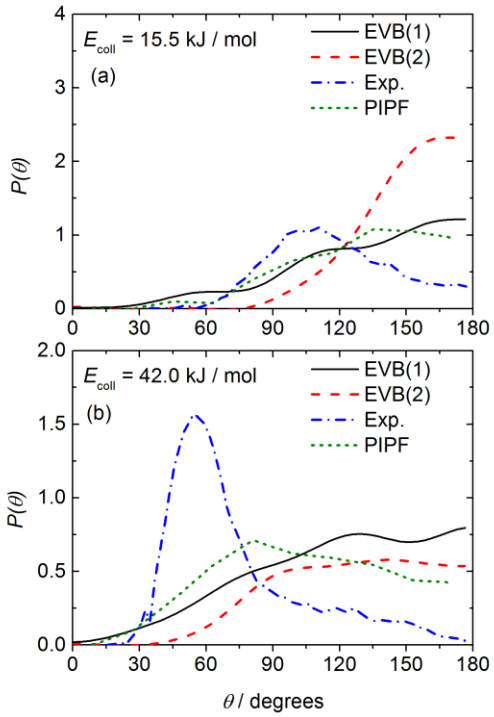

Figure 3: Comparison of computed and experimental $CH_4 + Cl \rightarrow CH_3(v=0) + HCl(v=0)$ differential cross sections in two collision energy regimes. The EVB(1) (black solid line) and EVB(2) (red dashed line) angular distribution functions from the current work are compared with experimental data and the QCT calculations of Czakó and Bowman (denoted PIPF for permutation invariant polynomial fitting) adapted from Ref.[26]. Panel (a) compares the distributions computed on the EVB(1) and EVB(2) PESs at a collision energy of 15.5 kJ mol^{-1} with the Czakó and Bowman calculations and experimental data at E_{coll} = 17.6 kJ mol^{-1}. The EVB-based trajectory calculations in panel (b) were conducted at a collision energy of 42.0 kJ mol^{-1} and are compared with the Czakó and Bowman calculations and experimental data at E_{coll} = 40.6 kJ mol^{-1}.

If the projection of the linear momentum onto the reaction coordinate is small, the system cannot climb up the steep potential energy wall to the TS, and is repelled without reaction having occurred. The EVB(1) DCS is more sideways scattered than that for EVB(2) which can be attributed to the lower TS energy and the shallower gradient of the exit channel wall.

The differential cross section is generally a sensitive probe of the forces acting on the system during the course of the reaction. Therefore, in order to assess the influence of the topography of the PES, DCSs were also calculated for both surfaces at a collision energy of 42.0 kJ mol^{-1} (Fig. 3(b)). At this higher collision energy, the HCl is sideways and backward scattered. There is a sufficient amount of linear momentum aligned along the reaction coordinate to surmount the barrier, even if its main component is not aligned along this direction. Hence, the final velocity of the HCl atom becomes more parallel to the initial velocity of the Cl atom. This result is in qualitative accordance with the experimental observations of Liu and coworkers.[26] However, experimental DCS are markedly more sideways and forward scattered than those reported in this work. The DCSs of Czakó and Bowman also predict more backwards scattering than the experimental measurements,[32] and the agreement is good between ours and their calculated distributions. The discrepancy between the QCT calculations and experimental measurements of the DCS is intriguing, and cannot be attributed to the effects of spin-orbit coupling because the PES of Czakó and Bowman incorporated this interaction. Perhaps a quantum mechanical effect not captured by the QCT calculations, such as tunnelling or a scattering resonance, is contributing to the experimental result.

Conclusions

The $CH_4 + Cl \rightarrow CH_3 + HCl$ hydrogen-abstraction reaction represents a challenging test case for the EVB method of describing a potential energy surface. The EVB formalism provides a computationally inexpensive framework to construct reactive PESs and perform classical dynamics calculations and our results suggest that it works well for this benchmark reaction. The potential energy surfaces obtained here are not as accurate as the best global fit potential energy surface reported in the literature, either in terms of root mean square error compared to the *ab initio* points, or in terms of the predicted dynamical behaviour in comparison to experiment. However, these new surfaces are obtained with

much less input from *ab initio* computation, relying instead on a good zeroth-order description of the reactants and products through the use of a molecular-mechanics type force-field.

High level *ab initio* calculations were carried out to determine the topography of the PES. Further *ab initio* points were used to parametrise the molecular mechanics force fields for degrees of freedom other than the reaction coordinate. Two reactive EVB PESs were generated, one by fitting to *ab initio* points sampled from C_{3v} geometries, the other including only energies computed for unconstrained geometries selected from trajectories. The properties of the stationary points of the EVB surfaces compare well with those obtained from the electronic structure calculations. Quasi-classical trajectory calculations were performed on both surfaces at collisions energies of 15.5 kJ mol^{-1} and 42.0 kJ mol^{-1}. The resultant rotational distributions were in reasonable agreement with the experimental data. Differential cross sections were also calculated that show the general characteristics of the experimentally observed scattering distributions, and which agree well with QCT calculations on a previously reported PES derived from a much larger set of *ab initio* energy points.[32]

The advantages of the EVB method are twofold. First, it provides a way to treat explicitly all degrees of freedom of the reactive system in a computationally undemanding way. This enhancement is achieved by using molecular mechanics forces. The consequent loss of accuracy can be ameliorated by refitting all, or the most important, energy terms in the force field. Second, the method allows us to construct various EVB PESs by including or excluding different reactant, product or intermediate diabatic PESs when constructing the EVB matrix. Although not used here, this flexibility can be exploited to gain insights on the effects of different parts of the PES on the dynamics of more complicated reactions. We now plan to harness these features of the EVB method to investigate other reactions, such as those between unsaturated hydrocarbons and halogens or pseudo-halogens (such as the CN radical) where direct abstraction and addition/elimination pathways compete.

Acknowledgements

We thank Prof Saulo Vázquez, Dr David Tew and Dr David Glowacki for insightful discussions. We thank Dr Gábor Czakó and Prof Joel Bowman for providing us with their calculated angular distribution functions. Funding from EPSRC Programme Grant EP/L005913/1 is gratefully acknowledged. GTD thanks EPSRC for funding for a studentship.

Supporting Information

Supporting information summarizes the functional forms used to describe molecular mechanics potentials, and the optimized values of parameters for these force fields and the EVB coupling terms. This material is available free of charge via the Internet at http://pubs.acs.org.

References

1. Eyring, H. The Activated Complex and the Absolute Rate of Chemical Reactions. *Chem Rev* **1935,** *17*, 65-77.
2. Eyring, H. The Activated Complex in Chemical Reactions. *J Chem Phys* **1935,** *3*, 107-115.
3. Eyring, H.; Polanyi, M. Concerning Simple Gas Reactions. *Z Phys Chem B-Chem E* **1931,** *12*, 279-311.
4. Bowman, J. M.; Schatz, G. C. Theoretical-Studies of Polyatomic Bimolecular Reaction Dynamics. *Annu Rev Phys Chem* **1995,** *46*, 169-195.
5. Nyman, G. Computational Methods of Quantum Reaction Dynamics. *Int J Quantum Chem* **2014,** *114*, 1183-1198.
6. Braams, B. J.; Bowman, J. M. Permutationally Invariant Potential Energy Surfaces in High Dimensionality. *Int Rev Phys Chem* **2009,** *28*, 577-606.
7. Truhlar, D. G. Valence Bond Theory for Chemical Dynamics. *J Comput Chem* **2007,** *28*, 73-86.
8. Fu, B. N.; Han, Y. C.; Bowman, J. M. Three-State Surface Hopping Calculations of Acetaldehyde Photodissociation to CH_3 + HCO on Ab Initio Potential Surfaces. *Faraday Discuss* **2012,** *157*, 27-39.
9. Xie, Z.; Bowman, J. M. Permutationally Invariant Polynomial Basis for Molecular Energy Surface Fitting Via Monomial Symmetrization. *J Chem Theory Comput* **2010,** *6*, 26-34.
10. Bowman, J. M.; Braams, B. J.; Carter, S.; Chen, C.; Czako, G.; Fu, B.; Huang, X.; Kamarchik, E.; Sharma, A. R.; Shepler, B. C., et al. Ab-Initio-Based Potential Energy Surfaces for Complex Molecules and Molecular Complexes. *J Phys Chem Lett* **2010,** *1*, 1866-1874.
11. Cheng, T. C.; Jiang, L.; Asmis, K. R.; Wang, Y. M.; Bowman, J. M.; Ricks, A. M.; Duncan, M. A. Mid- and Far-IR Spectra of H_5^+ and D_5^+ Compared to the Predictions of Anharmonic Theory. *J Phys Chem Lett* **2012,** *3*, 3160-3166.

12. Li, J.; Xie, C. J.; Ma, J. Y.; Wang, Y. M.; Dawes, R.; Xie, D. Q.; Bowman, J. M.; Guo, H. Quasi-Classical Trajectory Study of the HO+CO $\rightarrow$ H+CO_2 Reaction on a New Ab Initio Based Potential Energy Surface. *J Phys Chem A* **2012,** *116*, 5057-5067.
13. Ho, T. S.; Rabitz, H. Reproducing Kernel Hilbert Space Interpolation Methods as a Paradigm of High Dimensional Model Representations: Application to Multidimensional Potential Energy Surface Construction. *J Chem Phys* **2003,** *119*, 6433-6442.
14. Schatz, G. C.; Papaioannou, A.; Pederson, L. A.; Harding, L. B.; Hollebeek, T.; Ho, T. S.; Rabitz, H. A Global a-State Potential Surface for H_2O: Influence of Excited States on the O(^{1}D)+H_2 Reaction. *J Chem Phys* **1997,** *107*, 2340-2350.
15. Ischtwan, J.; Collins, M. A. Molecular-Potential Energy Surfaces by Interpolation. *J Chem Phys* **1994,** *100*, 8080-8088.
16. Nguyen, K. A.; Rossi, I.; Truhlar, D. G. A Dual-Level Shepard Interpolation Method for Generating Potential-Energy Surfaces for Dynamics Calculations. *J Chem Phys* **1995,** *103*, 5522-5530.
17. Frankcombe, T. J.; Collins, M. A. Growing Fragmented Potentials for Gas-Surface Reactions: The Reaction between Hydrogen Atoms and Hydrogen-Terminated Silicon (111). *J Phys Chem C* **2012,** *116*, 7793-7802.
18. Pruitt, S. R.; Addicoat, M. A.; Collins, M. A.; Gordon, M. S. The Fragment Molecular Orbital and Systematic Molecular Fragmentation Methods Applied to Water Clusters. *Phys Chem Chem Phys* **2012,** *14*, 7752-7764.
19. Warshel, A. Electrostatic Basis of Structure-Function Correlation in Proteins. *Accounts Chem Res* **1981,** *14*, 284-290.
20. Warshel, A.; Weiss, R. M. An Empirical Valence Bond Approach for Comparing Reactions in Solutions and in Enzymes. *J Am Chem Soc* **1980,** *102*, 6218-6226.
21. Kim, Y.; Corchado, J. C.; Villa, J.; Xing, J.; Truhlar, D. G. Multiconfiguration Molecular Mechanics Algorithm for Potential Energy Surfaces of Chemical Reactions. *J Chem Phys* **2000,** *112*, 2718-2735.
22. Murray, C.; Orr-Ewing, A. J. The Dynamics of Chlorine-Atom Reactions with Polyatomic Organic Molecules. *Int Rev Phys Chem* **2004,** *23*, 435-482.
23. Banks, S. T.; Clary, D. C. Reduced Dimensionality Quantum Dynamics of Cl+CH_4 $\rightarrow$ HCl+CH_3 on an Ab Initio Potential. *Phys Chem Chem Phys* **2007,** *9*, 933-943.
24. Shan, X.; Remmert, S. M.; Clary, D. C.; Zhang, B. L.; Liu, K. P. Crossed-Beam and Reduced Dimensionality Studies of the State-to-State Integral Cross Sections of the Cl + HCD_3(v) $\rightarrow$ HCl(v ') + CD_3 Reaction. *Chem Phys Lett* **2013,** *587*, 88-92.
25. Simpson, W. R.; Orr-Ewing, A. J.; Zare, R. N. State-to-State Differential Cross-Sections for the Reaction Cl($^2P_{3/2}$)+CH_4(ν_3=1,J=1) $\rightarrow$HCl(ν'=1,J')+CH_3. *Chem Phys Lett* **1993,** *212*, 163-171.
26. Zhang, B. L.; Liu, K. P.; Czako, G.; Bowman, J. M. Translational Energy Dependence of the Cl + CH_4(ν_b=0, 1) Reactions: A Joint Crossed-Beam and Quasiclassical Trajectory Study. *Mol Phys* **2012,** *110*, 1617-1626.
27. Kawamata, H.; Tauro, S.; Liu, K. Unravelling the Reactivity of Antisymmetric Stretch-Excited CH_4 with Cl by-Product Pair-Correlation Measurements. *Phys Chem Chem Phys* **2008,** *10*, 4378-4382.
28. Simpson, W. R.; Rakitzis, T. P.; Kandel, S. A.; Orr-Ewing, A. J.; Zare, R. N. Reaction of Cl with Vibrationally Excited CH_4 and CHD_3 - State-to-State Differential Cross-Sections and Steric Effects for the HCl Product. *J Chem Phys* **1995,** *103*, 7313-7335.
29. Wang, F. Y.; Lin, J. S.; Liu, K. P. Steric Control of the Reaction of CH Stretch-Excited CHD_3 with Chlorine Atom. *Science* **2011,** *331*, 900-903.
30. Yoon, S.; Henton, S.; Zivkovic, A. N.; Crim, F. F. The Relative Reactivity of the Stretch-Bend Combination Vibrations of CH_4 in the Cl($^2P_{3/2}$)+CH_4 Reaction. *J Chem Phys* **2002,** *116*, 10744-10752.
31. Yan, S.; Wu, Y. T.; Zhang, B. L.; Yue, X. F.; Liu, K. P. Do Vibrational Excitations of CHD_3 Preferentially Promote Reactivity toward the Chlorine Atom? *Science* **2007,** *316*, 1723-1726.
32. Czako, G.; Bowman, J. M. Dynamics of the Reaction of Methane with Chlorine Atom on an Accurate Potential Energy Surface. *Science* **2011,** *334*, 343-346.

33. Wang, F. Y.; Liu, K. P.; Rakitzis, T. P. Revealing the Stereospecific Chemistry of the Reaction of Cl with Aligned $CHD_3(v_1=1)$. *Nat Chem* **2012,** *4*, 636-641.
34. Yu, H. G.; Nyman, G. Reaction Dynamics of Chlorine Atom with Methane: Dual-Level Ab Initio Analytic Potential Energy Surface and Isotope Effects. *J Chem Phys* **1999,** *111*, 6693-6704.
35. Yu, H. G.; Nyman, G. A Four Dimensional Quantum Scattering Study of the $Cl+CH_4 \leftrightarrow HCl+CH_3$ Reaction Via Spectral Transform Iteration. *J Chem Phys* **1999,** *110*, 7233-7244.
36. Yu, H. G.; Nyman, G. Three-Dimensional Quantum Scattering Calculations on the $Cl+CH_4 \leftrightarrow HCl+CH_3$ Reaction. *Phys Chem Chem Phys* **1999,** *1*, 1181-1190.
37. Remmert, S. M.; Banks, S. T.; Harvey, J. N.; Orr-Ewing, A. J.; Clary, D. C. Reduced Dimensionality Spin-Orbit Dynamics of $CH_3 + HCl \leftrightarrow CH_4 + Cl$ on Ab Initio Surfaces. *J Chem Phys* **2011,** *134*, 204311.
38. Troya, D.; Weiss, P. J. E. Ab Initio and Direct Quasiclassical-Trajectory Study of the $Cl+CH_4 \rightarrow HCl+CH_3$ Reaction. *J Chem Phys* **2006,** *124*, 074313.
39. Greaves, S. J.; Rose, R. A.; Abou-Chahine, F.; Glowacki, D. R.; Troya, D.; Orr-Ewing, A. J. Quasi-Classical Trajectory Study of the Dynamics of the $Cl + CH_4 \rightarrow HCl + CH_3$ Reaction. *Phys Chem Chem Phys* **2011,** *13*, 11438-11445.
40. Castillo, J. F.; Aoiz, F. J.; Banares, L. Quasiclassical Trajectory Study of the $Cl+CH_4$ Reaction Dynamics on a Quadratic Configuration Interaction with Single and Double Excitation Interpolated Potential Energy Surface. *J Chem Phys* **2006,** *125*, 124316.
41. Collins, M. A. Molecular Potential-Energy Surfaces for Chemical Reaction Dynamics. *Theor Chem Acc* **2002,** *108*, 313-324.
42. Thompson, K. C.; Jordan, M. J. T.; Collins, M. A. Molecular Potential Energy Surfaces by Interpolation in Cartesian Coordinates. *J Chem Phys* **1998,** *108*, 564-578.
43. Thompson, K. C.; Jordan, M. J. T.; Collins, M. A. Polyatomic Molecular Potential Energy Surfaces by Interpolation in Local Internal Coordinates. *J Chem Phys* **1998,** *108*, 8302-8316.
44. Czako, G.; Bowman, J. M. Accurate Ab Initio Potential Energy Surface, Thermochemistry, and Dynamics of the $Cl(^2P, {}^2P_{3/2}) + CH_4 \rightarrow HCl + CH_3$ and $H + CH_3Cl$ Reactions. *J Chem Phys* **2012,** *136* 044307.
45. Troya, D.; Garcia-Molina, E. Quasiclassical Trajectory Study of the $O(^3P)+CH_4 \rightarrow OH+CH_3$ Reaction with a Specific Reaction Parameters Semiempirical Hamiltonian. *J Phys Chem A* **2005,** *109*, 3015-3023.
46. Rudic, S.; Murray, C.; Harvey, J. N.; Orr-Ewing, A. J. On-the-Fly Ab Initio Trajectory Calculations of the Dynamics of Cl Atom Reactions with Methane, Ethane and Methanol. *J Chem Phys* **2004,** *120*, 186-198.
47. Glowacki, D. R.; Orr-Ewing, A. J.; Harvey, J. N. Product Energy Deposition of CN Plus Alkane H Abstraction Reactions in Gas and Solution Phases. *J Chem Phys* **2011,** *134*, 214508.
48. Glowacki, D. R.; Rose, R. A.; Greaves, S. J.; Orr-Ewing, A. J.; Harvey, J. N. Ultrafast Energy Flow in the Wake of Solution-Phase Bimolecular Reactions. *Nat Chem* **2011,** *3*, 850-855.
49. Knizia, G.; Adler, T. B.; Werner, H. J. Simplified CCSD(T)-F12 Methods: Theory and Benchmarks. *J Chem Phys* **2009,** *130*, 054104.
50. Weigend, F.; Kohn, A.; Hattig, C. Efficient Use of the Correlation Consistent Basis Sets in Resolution of the Identity MP2 Calculations. *J Chem Phys* **2002,** *116*, 3175-3183.
51. Werner, H. J.; Knowles, P. J.; Knizia, G.; Manby, F. R.; Schutz, M. Molpro: A General-Purpose Quantum Chemistry Program Package. *Wires Comput Mol Sci* **2012,** *2*, 242-253.
52. Lancaster, P. On Eigenvalues of Matrices Dependent on a Parameter. *Numerische Mathematik* **1964,** *6*, 377-387.
53. Schlick, T. *Molecular Modeling and Simulation: An Interdisciplinary Guide*. Springer: New York, 2010.
54. Buckingham, R. A.; Corner, J. Tables of 2nd Virial and Low-Pressure Joule-Thomson Coefficients for Intermolecular Potentials with Exponential Repulsion. *Proc R Soc Lon Ser-A* **1947,** *189*, 118-129.

55. Chang, Y. T.; Miller, W. H. An Empirical Valence Bond Model for Constructing Global Potential-Energy Surfaces for Chemical-Reactions of Polyatomic Molecular-Systems. *J Phys Chem-US* **1990,** *94*, 5884-5888.
56. Dunning, G. T.; Glowacki, D. R.; Preston, T. J.; Greaves, S. J.; Greetham, G. M.; Clark, I. P.; Towrie, M.; Harvey, J. N.; Orr-Ewing, A. J. Vibrational Relaxation and Microsolvation of DF after F-Atom Reactions in Polar Solvents. *Science* **2015,** *347*, 530-533.
57. Hase, W. L.; Duchovic, R. J.; Hu, X.; Komornicki, A.; Lim, K. F.; Lu, D.-H.; Peslherbe, G. H.; Swamy, K. N.; Vande Linde, S. R.; Varandas, A. J. C., et al. *Venus96: A General Chemical Dynamics Computer Program*, 1996.
58. Bunker, D. L.; Hase, W. L. Non-RRKM Unimolecular Kinetics - Molecules in General, and CH_3NC in Particular. *J Chem Phys* **1973,** *59*, 4621-4632.
59. Hase, W. L.; Wolf, R. J.; Sloane, C. S. Trajectory Studies of the Molecular-Dynamics of Ethyl Radical Decomposition. *J Chem Phys* **1979,** *71*, 2911-2928.
60. NIST Chemistry Webbook, NIST Standard Reference Database Number 69 http://webbook.nist.gov. Series Editors, Linstrom, P. J.; Mallard, W. G.
61. Murray, C.; Retail, B.; Orr-Ewing, A. J. The Dynamics of the H-Atom Abstraction Reactions between Chlorine Atoms and the Methyl Halides. *Chem Phys* **2004,** *301*, 239-249.

Table of Contents Graphic